PERGAMON

Journal of Structural Geology 25 (2003) 159–169

JOURNAL OF STRUCTURAL GEOLOGY

www.elsevier.com/locate/jsg

Composite magnetic fabrics and *S–C* structure in granitic gneiss of Cerro de los Viejos, La Pampa province, Argentina

Renata N. Tomezzoli[a,*], William D. MacDonald[b], Hugo Tickyj[c]

[a]*CONICET, Universidad de Buenos Aires, Departamento de Ciencias Geológicas, F.C.E.yN., Ciudad Universitaria, Pabellón II C1428EH, Buenos Aires, Argentina*

[b]*State University of New York at Binghamton, Department of Geological Sciences. Binghamton, NY 13902-6000, USA*

[c]*Universidad Nacional de La Pampa, F.C.E.yN., Departamento de Ciencias Naturales., Av. Uruguay 151, 6300 Santa Rosa, La Pampa, Argentina*

Received 20 December 2001; received in revised form 10 January 2002; accepted 11 January 2002

Abstract

The Cerro los Viejos gneiss, in La Pampa Province, Argentina, is a mylonitized granite which lies along the late Paleozoic deformed boundary zone between the Patagonia block and 'mainland' Gondwana to the north. Petrofabric and anisotropy of magnetic susceptibility (AMS) analyses were compared for this body. Unexpectedly, it was found that the K_{min} poles deviate from the poles of the main foliation s_1 by about 25°. Similarly, but not so noticeably, the K_{max} poles trend NE/SW, with a near-horizontal plunge, whereas the principal lineation l_1 plunges gently SW. This unusual situation is attributed to the existence of superimposed fabrics arising from *S–C* structures. Examination of oriented cores in a modified universal stage and of oriented thin-sections revealed that the K_{min} poles are clearly associated with a younger but less obvious metamorphic '*C*' foliation (s_2). Biotite and magnetite, the main contributors to the AMS response, are distributed along both s_1 and s_2. The dominance of s_2 in the AMS anisotropy suggests that magnetite is preferentially distributed on s_2.

Keywords: Petrofabric; Anisotropy of magnetic susceptibility; *S–C* structure; Gondwana; Granitic gneiss; Argentina

1. Introduction

A study of the emplacement, fabric and structures of the mylonitic–granitic pluton of Cerro de los Viejos, in La Pampa province, Argentina, was carried out to reconstruct the kinematics of an area along the southwestern margin of Gondwanaland (Fig. 1). Anisotropy of magnetic susceptibility (AMS) is an effective tool for analysing fabrics in granitic rocks, with the potential to identify the orientations of the principal axes of finite strain to which the rocks were subjected (Graham, 1954; Borradaile, 1988). Composite magnetic fabrics can reveal multiple deformation episodes in granitic and metamorphic rocks, and may depart from the orientations of both s-plane and c-plane (Bouchez and Gleizes, 1995; Aranguren et al., 1996; Werner and Borradaile, 1996; Borradaile and Henry, 1997; Benn et al., 1998; Trindade et al., 1999).

The intensity of the magnetic susceptibility (K) is the sum of the diamagnetic, paramagnetic, antiferromagnetic and ferromagnetic responses of constituent minerals (e.g. Gleizes et al., 1993). Of these, the diamagnetic response is typically very weak, and opposes the applied field; this response is contributed by iron-free silicates such as quartz and feldspar. The paramagnetic contribution is carried by Fe-bearing silicates (Rochette, 1987), which, in granitoids, includes the phyllosilicates (biotite, chlorite, Fe-muscovite), amphiboles, ilmenite, pyroxene, cordierite, garnet and tourmaline. The antiferromagnetic contribution, typically provided by hematite and goethite, is negligible in practice. The ferromagnetic contribution is commonly a major component and is associated with magnetite and occasionally with sulphides such as pyrrhotite (Jover et al., 1989; Gleizes et al., 1993). In deformed granitic rocks, deformation may control the orientation of ferromagnetic minerals. The AMS response in such rocks typically reflects the preferred crystallographic orientation of iron-bearing silicates and the shape and distribution of magnetite grains. In the present study, several properties were used to analyse the magnetic mineralogy: isothermal remanent magnetization (IRM) acquisition, mean susceptibilities, and remanence change with temperature.

The Cerro de los Viejos (CLV) is located north of the Colorado River in south-central Argentina (Fig. 1a).

* Corresponding author. Tel./fax: +54-11-4576-3329.
E-mail address: renata@gl.fcen.uba.ar (R.N. Tomezzoli).

0191-8141/02/$ - see front matter
PII: S0191-8141(02)00030-5

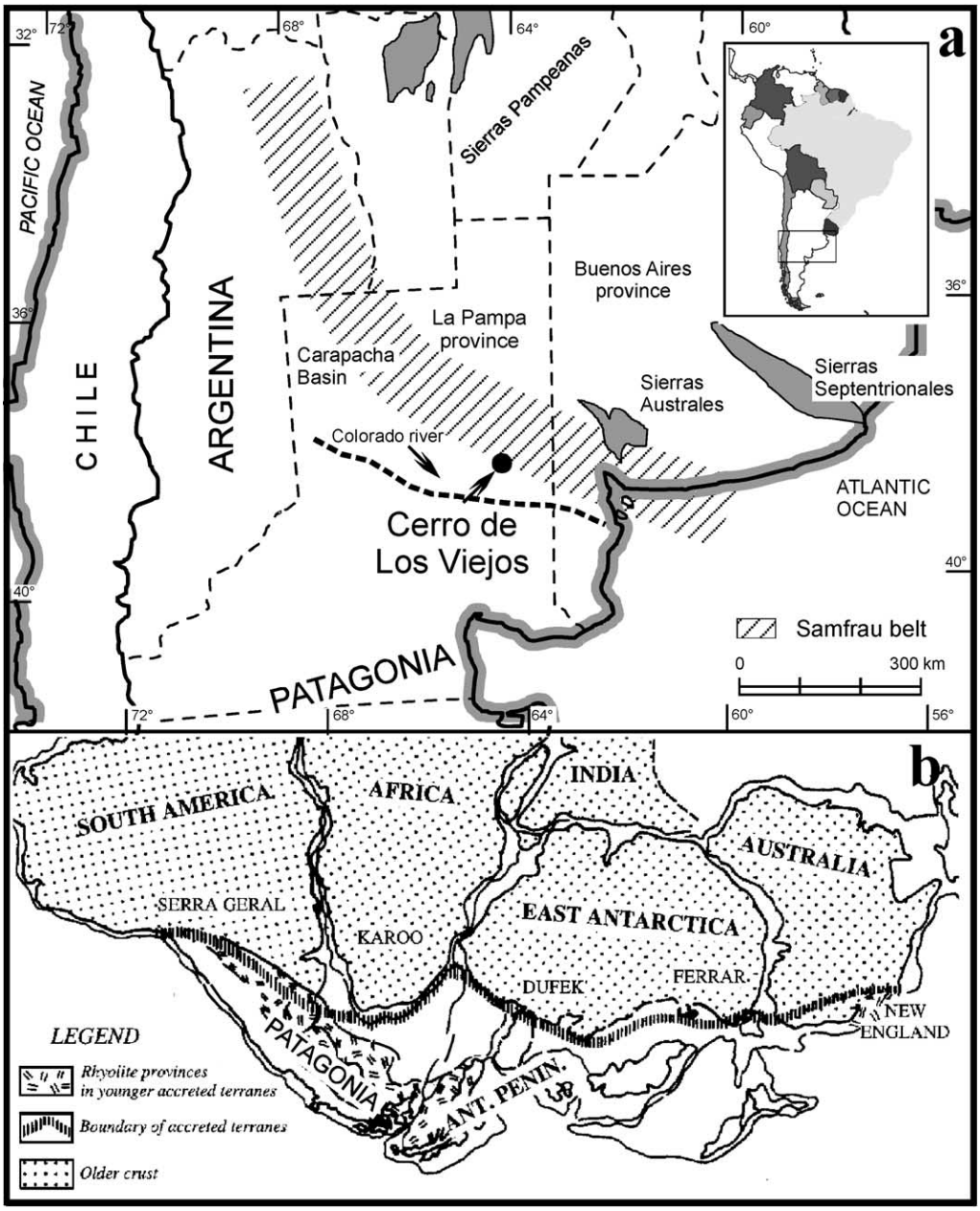

Fig. 1. Location of the study area. The granitic orthogneiss complex of Cerro de los Viejos includes the Cerro de los Viejos, Monte Redondo and Tres Hermanas, in southeastern La Pampa province, Argentina, exposed in the orogenic belt known as 'Samfrau Geosyncline' (Du Toit, 1927). (b) Modified from Kay et al., 1989.

According to Ramos (1984), an ocean was consumed by subduction towards Patagonia along the northern boundary of Patagonia at the southern margin of Gondwana (Fig. 1b), before the continental blocks collided in the mid to late Paleozoic. Associated with this collision, and perhaps continuing for a period thereafter, deformation in the Sierras Australes (east of Cerro de los Viejos; Fig. 1) may have started in mid-Paleozoic to Permian (Tomezzoli and Vilas, 1999; Tomezzoli, 2001). The granitic and mylonitic gneisses of Cerro de los Viejos are part of a ductile shear zone related to this collisional orogen. Deformation is attributed to NE–SW directed compression (Tickyj and Llambías, 1994; Tickyj et al., 1997). It has been proposed that the northern boundary of the Patagonia block has been the locus of strike slip faulting (Rapalini and Vizán, 1993). Lateral slip along that zone should thus be recorded in near-horizontal lineations with trends near WNW/ESE, parallel to the boundary. Although shallow-plunging lineations are observed at Cerro de los Viejos, the trends are approximately orthogonal to the Patagonia boundary zone. Unless large rotations of the CLV body have occurred, the lineations preserved do not support the hypothesis of strike-slip displacement along the Patagonia boundary zone. The main objective of this integrated study of AMS, petrographic and

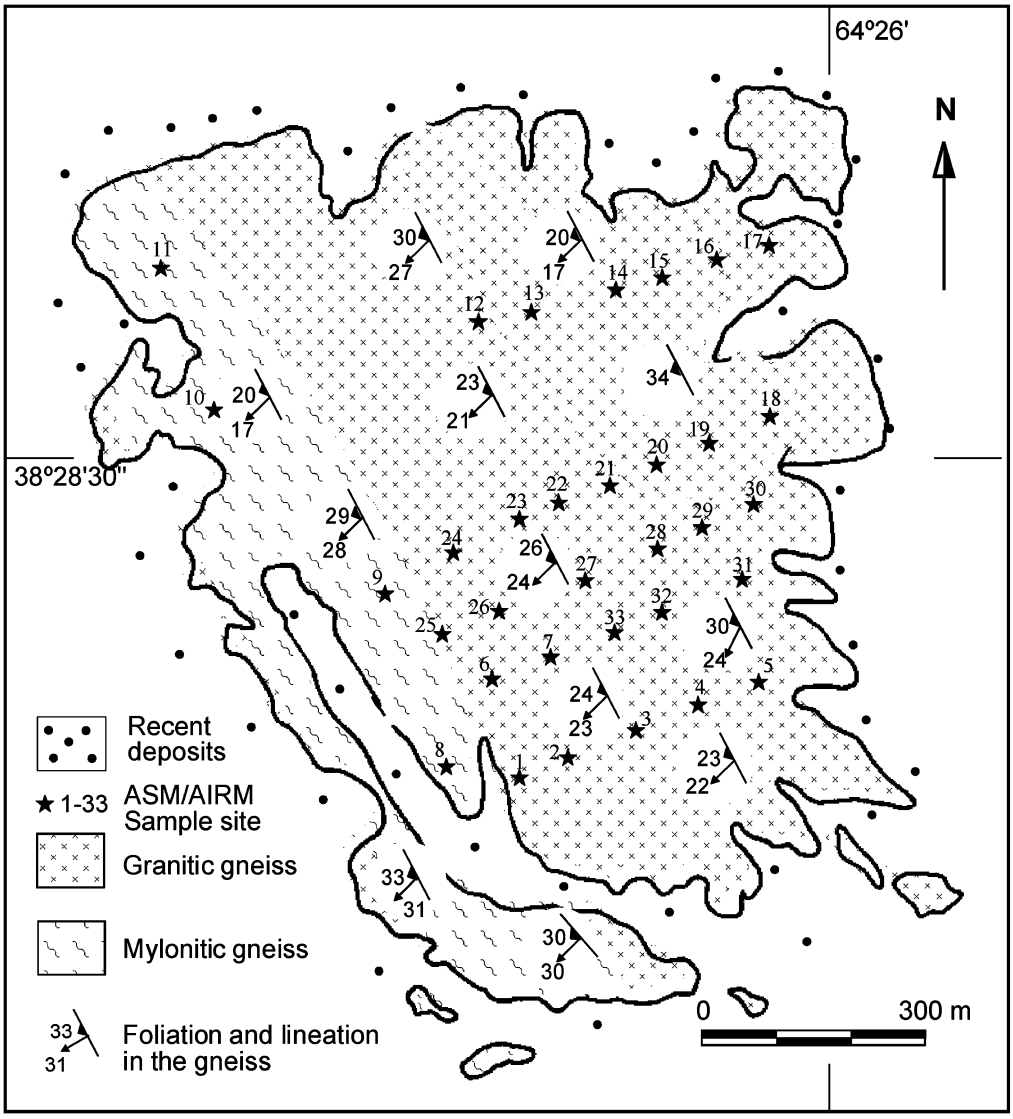

Fig. 2. Structural map of the Cerro de los Viejos (after Tickyj et al., 1997) and location of the sampling sites.

structural features is to investigate the kinematic history of this area, and to distinguish multiple tectonic events that account for the fabrics of the outcropping rocks.

2. Geological setting

The CLV belongs to the igneous–metamorphic basement considered by Linares et al. (1980) as the southward prolongation of the Sierras Pampeanas (Fig. 1). Granitic gneisses located in CLV and in the nearby Monte Redondo and Tres Hermanas were assigned by Tickyj (1999) to the Granitic Orthogneiss Complex. The CLV granite body forms an elliptical isolated outcrop, 1.5 km by 1 km, in an area of very low relief characterized by recent sedimentary deposits. The granite shows varied deformational features, with two well-defined structural domains having a gradational contact: a slightly foliated orthogneiss (or granitic gneiss) and a mylonitic gneiss (Fig. 2). In both structural domains coarse and fine-grained rock types, ascribed to differences in the protolith (Tickyj et al., 1997), can be distinguished.

A microscopic study of the CLV gneiss reveals the existence of two ductile deformation events. The principal foliation (s_1) is prominent in the outcrops. It is defined by the parallelism of lenticular grains and aggregates of feldspar and quartz. S_1 is penetrative throughout the granite, with an average strike 146° and average dip 27°SW (Fig. 3), and is synchronous with a regional medium grade metamorphism. S_1 is best developed in the mylonitic gneiss, and gradually decreases into the orthogneiss. In some places the granitic gneiss is richer in quartz, and the contacts between fine and coarse grained domains form narrow, well-foliated zones, typically with a well-defined mineral lineation (l_1) plunging 25° towards 222°. This lineation is marked by aligned recrystallized quartz–feldspar–mica aggregates and tourmaline (Fig. 4).

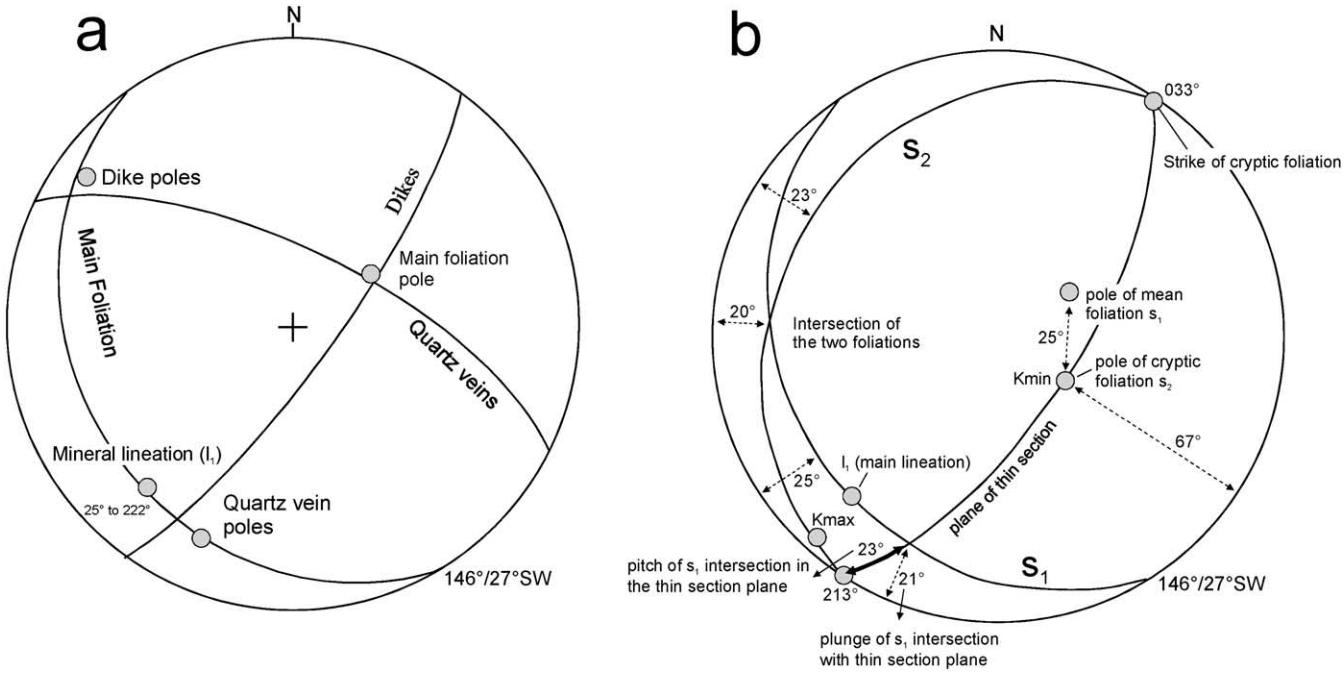

Fig. 3. (a) Principal petrofabric elements of the Cerro de los Viejos gneiss form an orthogonal set of foliation, quartz veins and dikes. Structural data from Tickyj et al. (1997). (b) Mean magnetic fabric elements: K_{max} and K_{min} are shown in relation to principal mesoscopic fabric elements (main foliation = s_1 and lineation = l_1). K_{min} is about 25° from the main mesoscopic foliation s_1 pole. K_{min} suggests the presence of a secondary foliation s_2, which was verified petrographically.

In the coarse-grained mylonitic gneiss, Type I *S*–*C* structures (Lister and Snoke, 1984) are developed, with sigmoidal asymmetric K-feldspar porphyroblasts indicating top-to-the-NE thrusting. K–Ar ages in biotite gave 304 ± 15 and 330 ± 15 Ma (Linares et al., 1980) and K–Ar and Rb–Sr ages obtained in muscovite that crystallized during this event are: 359.5 ± 3; 280.4 ± 2.3; 261 ± 13; 265 ± 13 Ma, constraining the timing of the deformation near the Carboniferous–Permian boundary (Tickyj, 1999).

The younger foliation (s_2) is secondary both in terms of relative age and in degree of development, and is only observed locally. S_2 is attributed to NNE striking shear zones dipping 30°WNW. The average orientation is 213°/39°NW. An angle of about 25° separates s_1 and s_2, and their intersection plunges 20° towards 276° (Fig. 3). Secondary structures in the CLV are represented by orthogonal quartz veins (296°/68°NE) truncated by undeformed granitic and pegmatitic dikes (036°/78°SE; Fig. 3).

3. AMS—directional data

AMS measurement can be expressed by a second-rank tensor where eigenvectors/eigenvalues are geometrically represented as an ellipsoid. The shapes and orientations of these ellipsoids can be related to magmatic flow in igneous rocks and kinematics of deformation in metamorphic rocks (Tarling and Hrouda, 1993). Commonly the flattening of the AMS ellipsoid (plane perpendicular to K_{min}) is parallel to the foliation in the rock, and the elongation of the ellipsoid (K_{max}) is parallel to the fabric lineation. CLV specimens were measured using the standard 15-position procedure with the Kappabridge KLY-2 (Geofyzika Brno) apparatus to obtain the magnitudes and orientations of K_{max}, K_{int} and K_{min}.

AMS results from 33 sites are combined in Fig. 5, from five traverses perpendicular to the mesoscopic structures (Fig. 2). Two to four hand samples were collected per site and oriented in the field using a magnetic compass. Four cores were drilled in each hand sample and two standard cylindrical specimens (22 mm long × 25 mm diameter) were taken from each core. Approximately 10 specimens per site were measured (Table 1).

Overall, the AMS signatures are predominantly triaxial (19 of 33 sites), with well-defined axial groups and relatively small uncertainty ovals about the means. Nine sites exhibit oblate tendencies, and only a few are prolate (Fig. 6, sites CV26, 29, 33). The remaining sites have too few data to be properly characterized.

AMS studies reveal that K_{max} is commonly parallel to a major lineation, but sometimes is parallel to the intersection line of two foliations (MacDonald and Ellwood, 1987). In the present case, the K_{max} axes plunging 06° towards 222° (Figs. 3 and 4) are far from the intersections of s_1 and s_2 (20° towards 276°; Fig. 3). The K_{max} axes are influenced by the mineral lineation trend and do not appear to represent an intersection lineation. In 22 sites, K_{max} plunges gently to the SW, close to l_1 (222°/25°; trend of the field-measured

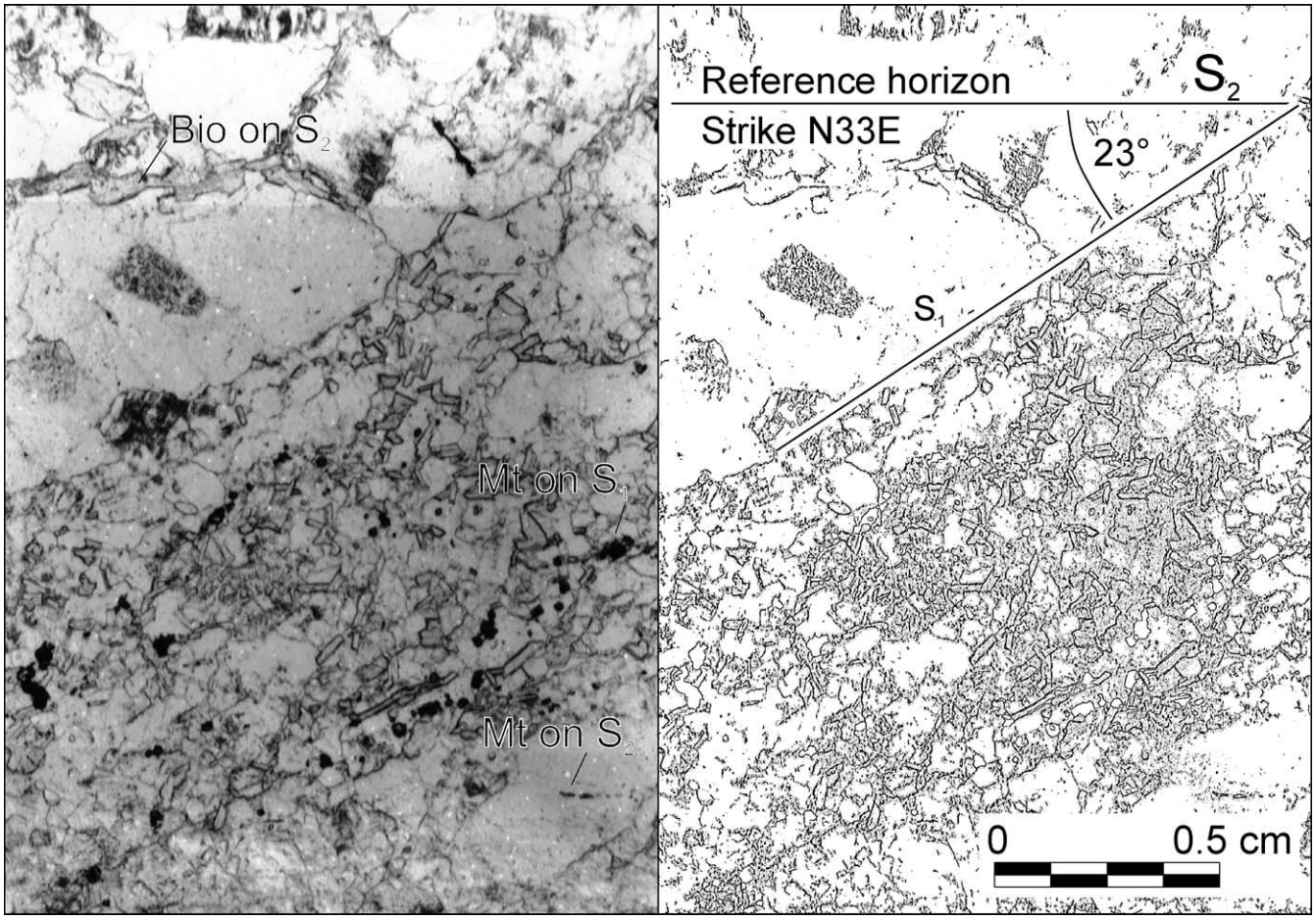

Fig. 4. Photomicrograph illustrates relationships of s_2 traces (horizontal) to s_1 traces (down to left) as seen in oriented thin sections. A horizontal line has an azimuth of 033°; the thin section plane dips 67°SE, so the view direction is inclined down 23° towards azimuth 303° (see Fig. 3b). Biotite plates and aggregates, magnetic oxide clusters and sheared tourmaline aggregates are parallel to s_2 and lie horizontal in this view of the thin section. Some biotite (bio) and magnetite (mt) also parallel s_1.

lineation; Fig. 3). The same K_{max} trend is observed in seven additional sites, but the plunge is in the opposite direction (Figs. 5 and 6: CV2, 8, 9, 16, 19, 25, 28). In three sites, the mean K_{max} plunges towards the N or NW (CV12, 23, 27). Mineral lineations are not recorded in the field from the NW-trending mylonitic gneiss zone. The four sites located in that zone (Figs. 2 and 6), all show the more or less SW/NE K_{max} axes. This argues against a strike-slip displacement along this zone, for which a horizontal lineation of trend 146°/326° is expected.

Contrary to expectations, the AMS mean K_{min} axis (123°/67°) does not agree well with the mean petrofabric foliation pole (Figs. 3 and 5) but corresponds best to the secondary foliation s_2. A site-by-site inspection shows that in only nine sites there is reasonably good agreement between K_{min} and the s_1 pole (Fig. 6; sites: CV1, 6, 7, 8, 12, 14, 17, 20, 24). In most sites (20 of 33), the s_2 to which K_{min} corresponds is a gently NW dipping plane. Because the s_1 and s_2 magnetic foliations intersect at about 25°, and because K_{max} is constrained to be orthogonal to K_{min}, then K_{max} cannot be exactly parallel to the mineral lineation l_1 of the main foliation. The T vs. P_j diagram (Jelinek 1981; Fig. 7) reveals an anisotropy degree mainly below 3%, with an ellipsoid more oblate than prolate.

The specimens display natural remanent magnetization (NRM) intensities between 5 and 2000 mA/m. The thermal demagnetization curve of composite IRM shows abrupt drops at 300 °C and near 575 °C (Fig. 8a). This thermal behavior and the loss of remanence intensity during AF demagnetization indicates that the magnetization is mostly carried by magnetite with a large contribution of multi-domain titanomagnetite. Presence of a high coercivity mineral fraction, probably hematite, is indicated by the failure to reach saturation at 1 T (Fig. 8b) in isothermal remanent magnetization (IRM) acquisition experiments.

4. Petrofabric analysis

Five specimens from each of the 33 sites were measured to study the orientation of the foliation,

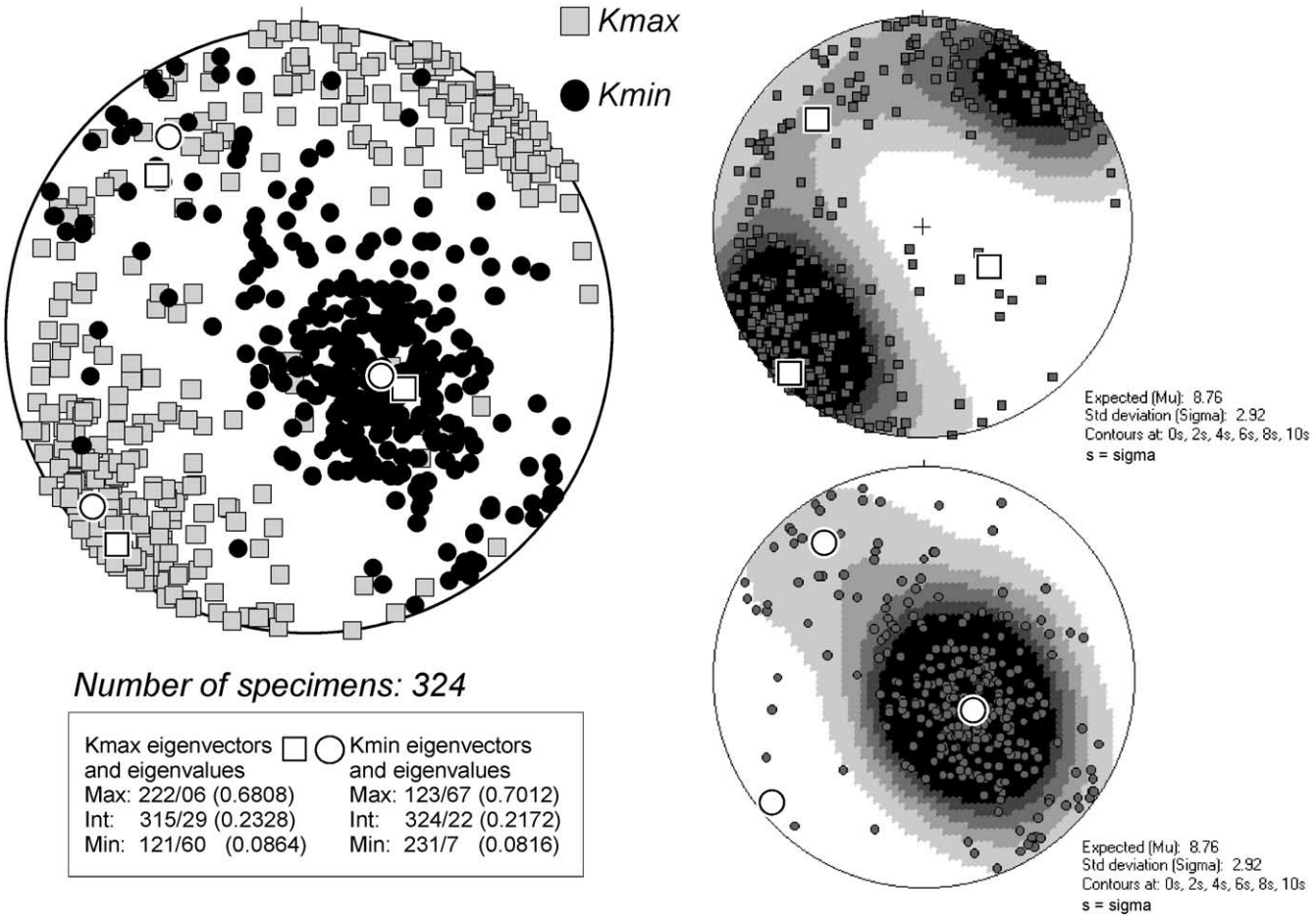

Fig. 5. Anisotropy of magnetic fabric results from Cerro de los Viejos. Stereographic projection of the three principal susceptibility ellipsoid axes for 324 specimens. Kamb density contours of specimen eigenvectors are given. Maximum cluster of K_{min} axes is in SE quadrant, away from the s_1 foliation poles in the NE quadrant (see Fig. 3) and indicates the presence of a cryptic foliation revealed in oriented thin-sections. Specimen K_{max}, and K_{min} axes were separately subjected to eigenvector analysis and their distributions and eigenvalues (normalized to one) are given in the box.

using a jig mounted in a standard 4-axis U-stage, and compared with the field measured foliations (Fig. 6). Mineral lineations, although visible in the field, were not apparent in the core specimens and were not measured with the U-stage. The mean foliation from the U-stage core measurements was estimated in two ways: (1) visually, from stereographic plots, and (2) analytically, by eigenvector analysis. In 28 of 33 sites, the poles of the minimum eigenvector and of the visually estimated mean foliation pole were coincident within a few degrees. In the other five sites, foliation in the cores was too faint to be measured accurately.

To explore the significance of the cryptic AMS foliation s_2, oriented thin-sections orthogonal to s_2 were cut from several cores (Fig. 4) for which the K_{min} axis was known to lie close to the center of the principal K_{min} cluster (Fig. 5). The plane of the thin-section was marked by a line around each core. The cores were oriented individually in a jig placed in the 4-axis U-stage and restored to their field orientation. A protractor with a rotatable circle (Rotangle^{TM}) was convenient to adjust the inclination angle of the core in the U-stage. A thin-section plane perpendicular to the cryptic foliation has the same strike as the cryptic foliation but is perpendicular to it; the thin-section plane therefore strikes 033° and dips 67°SE (Figs. 3 and 4). To mark that plane, the core was oriented in the U-stage with the desired thin-section plane vertical. A line marking a vertical plane intersecting the core was then inked around the core using a right-triangle as a drawing guide. The ends of a horizontal line in that plane were also marked. This line represents the line of strike and also helps to identify the intersection of s_2 with the plane of the thin-section. After cutting the core and preparing the thin-section blank, a line was scribed across the face of the blank to mark the orientation of the horizontal line (line of strike of cryptic foliation) in the plane of the thin-section. This line is a visible reference lineation under the petrographic microscope. All thin sections were prepared with the horizontal line rotated to the E–W position in the standard petrographic microscope. The view direction is 23° down towards azimuth 303°; i.e. down the dip of the plane

Table 1
Mean anisotropy of magnetic susceptibility (AMS) parameters. N: Number of specimens per site; $K_{mean} = (K_{max} + K_{int} + K_{min})/3$: bulk volume susceptibility in SI units; $L = K_{max}/K_{int}$: lineation; and $F = K_{int}/K_{min}$: foliation (Flinn 1962); $P = (K_{max}/K_{min})$: degree of anisotropy (Nagata, 1961); $T = 2(\ln(K_{int}/K_{min})/\ln(K_{max}/K_{min})) - 1$: Jelinek's shape parameter (Jelinek, 1981); dec. and inc. give the declination (azimuth) and inclination (plunge) of the K_{max} and K_{min} axes

Site	N	K_{mean} ($\times 10^{-4}$)	Mean AMS parameters				Mean eigenvectors	
			L	F	P	T	K_{max} Dec/inc	K_{min} Dec/inc
CV1	8	1.06	1.0011	1.0109	1.0120	0.8161	209/11	087/71
CV2	8	1.37	1.0077	1.0120	1.0198	0.2212	036/08	170/79
CV3	12	0.95	1.0146	1.0254	1.0404	1.0032	005/13	142/73
CV4	12	1.63	1.0070	1.0060	1.0131	1.0015	045/3	140/58
CV5	17	0.44	1.0024	1.0050	1.0075	0.3530	022/25	146/50
CV6	12	0.91	1.0086	1.0103	1.0190	0.0907	215/12	066/77
CV7	6	0.76	1.0054	1.0100	1.0154	0.2930	211/09	347/78
CV8	11	0.93	1.0068	1.0118	1.0187	0.2652	227/06	028/84
CV9	9	1.29	1.0218	1.0090	1.0309	−0.4137	043/11	146/49
CV10	10	0.64	1.0037	1.0110	1.0147	0.4924	197/01	104/76
CV11	3	7.09	1.0096	1.0097	1.0194	0.0048	237/12	339/43
CV12	17	1.83	1.0024	1.0466	1.0491	0.8997	193/08	296/60
CV13	9	0.87	1.0143	1.0046	1.0190	−0.5127	212/15	324/54
CV14	8	2.66	1.0055	1.0151	1.0207	0.4622	251/4	153/65
CV15	5	0.4	1.0082	1.0237	1.0321	0.4852	049/07	142/25
CV16	12	3.82	1.0375	1.0335	1.0722	−0.0555	232/05	141/01
CV17	17	1.2	1.0058	1.0075	1.0134	0.1245	247/30	73/60
CV18	8	1.11	1.0074	1.0250	1.0325	0.5422	027/10	140/65
CV19	12	1.08	1.0116	1.0163	1.0282	0.1673	038/22	155/49
CV20	9	0.72	1.0031	1.0144	1.0176	0.6442	018/03	114/63
CV21	12	0.57	1.0088	1.0180	1.0269	0.3417	033/03	126/47
CV22	13	0.29	1.0169	1.0191	1.0363	0.0603	243/27	152/02
CV23	9	1.97	1.0013	1.0169	1.0182	0.8560	023/13	134/58
CV24	10	0.28	1.0027	1.0131	1.0158	0.6561	232/30	090/53
CV25	7	2.17	1.0122	1.0176	1.0301	0.1784	026/07	130/63
CV26	8	1.68	1.0076	1.0013	1.0089	−0.7034	023/04	118/55
CV27	8	0.34	1.0090	1.0329	1.0422	0.5675	354/20	162/70
CV28	8	1.17	1.0145	1.0082	1.0228	−0.2773	041/21	181/63
CV29	9	1.02	1.0287	1.0145	1.0436	−0.3254	238/06	137/62
CV30	7	1.28	1.0072	1.0141	1.0213	0.3253	201/02	107/61
CV31	9	0.88	1.0336	1.0362	1.0710	0.0367	236/00	145/54
CV32	6	0.71	1.0104	1.0106	1.0211	0.0101	220/25	118/22
CV33	3	1.25	1.0082	1.0052	1.0134	−0.2241	262/15	017/60

of the cryptic foliation. Thus, any plane in the thin-section oriented parallel to the cryptic foliation s_2 will have its trace parallel to the scribed horizontal reference line. Also, in this view, the apparent dip of the visible foliation s_1 is down approximately 23° on the left, relative to the E–W horizontal reference line (Figs. 3 and 4); i.e. the pitch of s_1 in the plane of the thin-section, relative to the horizontal line of strike of s_2.

Several features were found to lie parallel to the trace of the cryptic foliation s_2 (Figs. 3 and 4): (1) trains of second generation opaque oxides, mainly in the 3–30 μm size range, which are also found parallel to the principal foliation trace; (2) parallel mica plates of both muscovite and biotite, which are more commonly parallel to s_2 than to s_1; (3) lenticular aggregates of quartz and feldspar, with a finer grain size than that of the predominant foliation s_1; (4) small quartz veins up to 3 mm thickness; and (5) trains of tourmaline with lilac pleochroism.

5. Discussion

The AMS study performed on the CLV mylonitic gneiss showed a good agreement between the K_{max} axis and the average mineral lineation trends (Figs. 3 and 5). However, K_{max} plunges more gently than the observed mineral lineation. The K_{min} axes, which might be expected to lie near the foliation poles, in the NE quadrant, lie mainly in the SE quadrant (Fig. 5). These two poles are about 25° apart (Fig. 3). Thus we have a somewhat unusual situation, in which an early strong mineral lineation controls the trend of K_{max}, and a weaker secondary foliation controls the orientation of K_{min} axes. In two sites, K_{min} axes are nearly horizontal, thus representing nearly vertical planes. K_{min} axes define a broad girdle from NW to SE, indicating dips for the K_{max}–K_{int} plane ranging from 0 to 90°. The mean K_{min} axis does not correlate well with the mean foliation pole, which lies in the NE quadrant, although for a few sites K_{min}

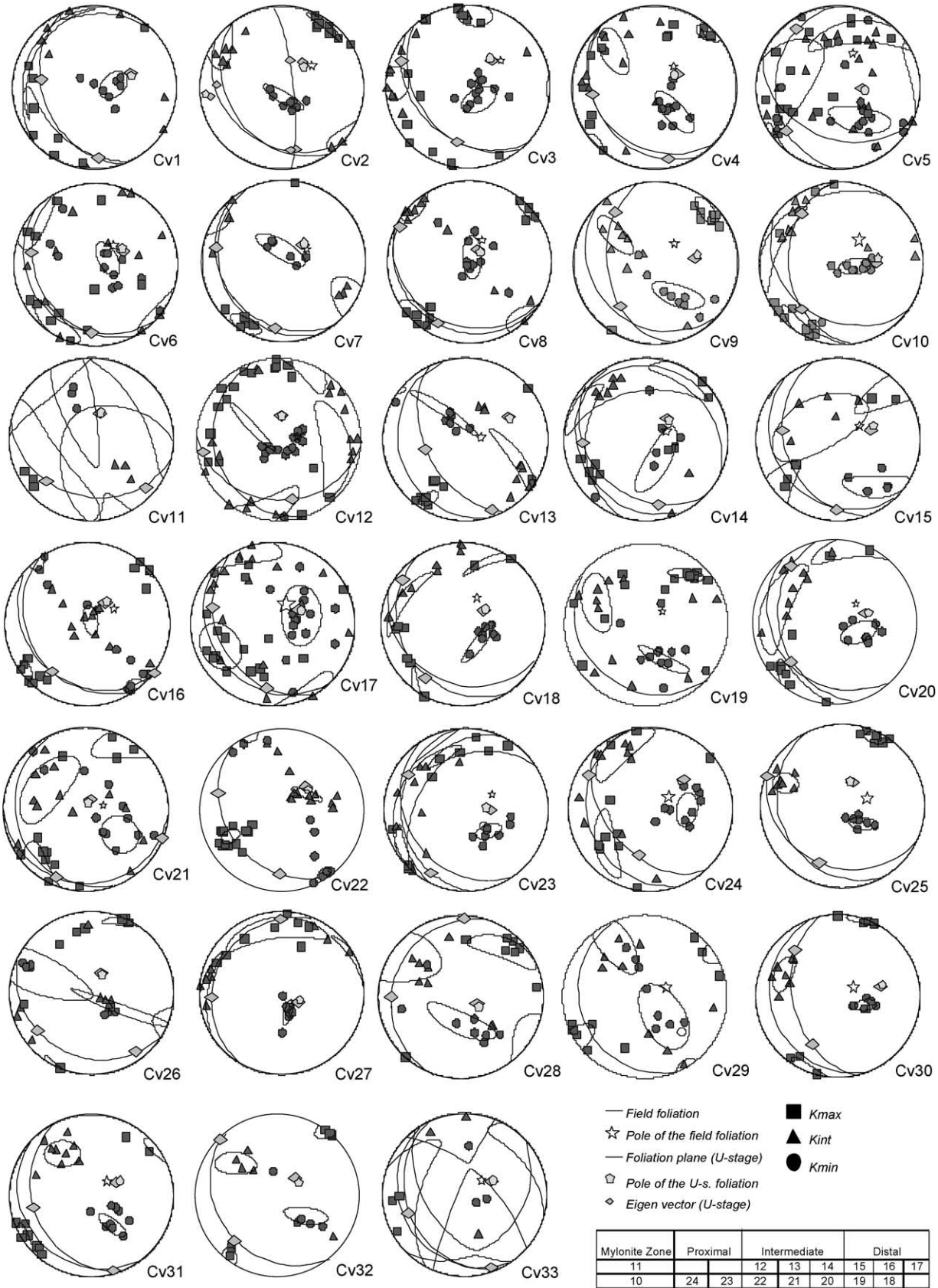

Mylonite Zone	Proximal		Intermediate			Distal		
11			12	13	14	15	16	17
10	24	23	22	21	20	19	18	
9	26		27	28	29	30		
25	6	7	33	32	31			
	1	2	3	4	5			

Fig. 6. Equal area stereoplots for 33 sites in which the axial directions K_{max}, K_{int} and K_{min} are plotted as squares, triangles and circles, respectively, together with their associated error ellipses. Structural data are also included for each individual site.

does correspond to that megascopic foliation. No major difference in AMS patterns was noticed between the mylonitic zone and the main granitic gneiss.

The AMS K_{min} axes for the CLV granitic gneisses clearly indicate the presence of a cryptic foliation which was not obvious in the field. This cryptic foliation is a secondary, weaker foliation, marked by oriented micas and opaque oxides which contribute to the AMS signatures of the rock. The results indicate that the AMS ellipsoid axes lie parallel to the general trend of the primary lineation. For AMS, the K_{max} axes are aligned along that trend (NE/SW or approximately 040° and 220°).

Normally, K_{min} poles lie close to foliation poles. In these rocks however, the K_{min} poles are in the SE quadrant, and the foliation poles are in the NE quadrant. Although the NE–SW trend of the K_{max} axes is parallel to the predominant lineation, the K_{max} axes are also anomalous as they are more gently plunging than the lineations, and even have opposite plunges, to the NE. The explanation probably involves distribution of paramagnetic minerals and ferromagnetic oxides in a plane dipping gently NW, oblique to the visible SW dipping foliation. This pattern implies the presence of a secondary foliation, for example the *C* plane of a *S–C* pair. This inference is supported by the petrographic examination of the oriented thin-sections.

The eigenvector analysis of foliations measured on the U-stage yielded results consistent with the field foliation (Fig. 6). In 16 of 33 sites, the minimum eigenvector for the foliations measured on the U-stage plunges gently SW. This represents the least moment of inertia for the foliation perpendiculars, which in other occurrences, is typically parallel to fold axes where folding is present. This pattern suggests that a low-amplitude ondulation is present in the core foliations. The fold axes of this foliation are parallel to the field-measured lineations. It is interesting that the pole of the great circle of K_{min} axes for 324 specimens (Fig. 5) also plunges gently SW, suggesting a folding pattern similar to that evident in the U-stage measurements. Thus, the K_{min} pattern is basically related to the lineation and to the fold axes of the foliations. However, the main clustering of the K_{min} poles in the SE quadrant is related to the secondary foliation s_2. In superimposed fabrics such as the *S–C* fabrics which are presented here, there arises the possibility that some surfaces may be heterogeneous features which do not contribute uniformly to the AMS response of a specimen (Borradaile and Tarling, 1981). This is not a problem in the present situation because s_2 foliations, although somewhat discontinuous, have a spacing of approximately 1 mm (Fig. 4). Also we estimate that the number of magnetite grains is at least of the order of thousands of grains in a single specimen, and they are prominently distributed along s_2.

One of the sites produced an unusual result (site 12, Fig. 6). The mean K_{min} axis and error oval for this site are clearly displaced from the distribution of K_{min} axes; the former are in the NW quadrant and the latter are mainly in the SE quadrant. Possibly this is a result of analysing a bimodally distributed axial population under the assumption that the distribution is unimodal. The K_{min} axis suggests the presence of two foliations, one dipping gently WNW and the other dipping gently NE. Such a bimodal distribution might result from a single foliation by sampling, for example, opposite limbs of a small fold or across a fault.

The thin-section examination revealed that biotite is preferentially but not exclusively oriented parallel to s_2 (Fig. 4). The fact that K_{min} axes lie in the same region suggests that iron oxides are preferentially scattered in the plane of s_2. Thin-section examination revealed that iron

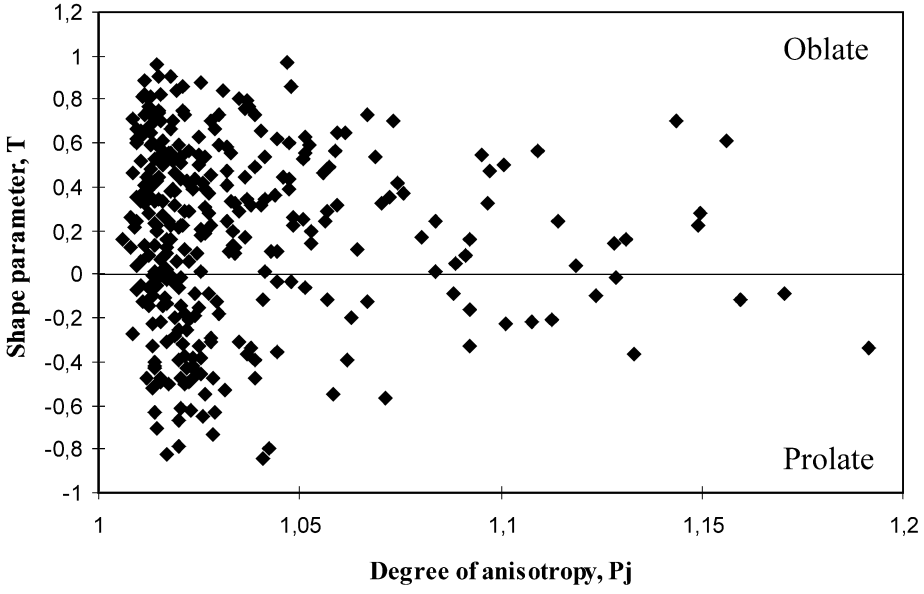

Fig. 7. Graph of *Pj–T* of AMS parameters of Jelinek (1981) shows wide range of shape parameters from prolate to oblate, with anisotropy degree mainly near 3% (1.03) but ranging up to almost 20%.

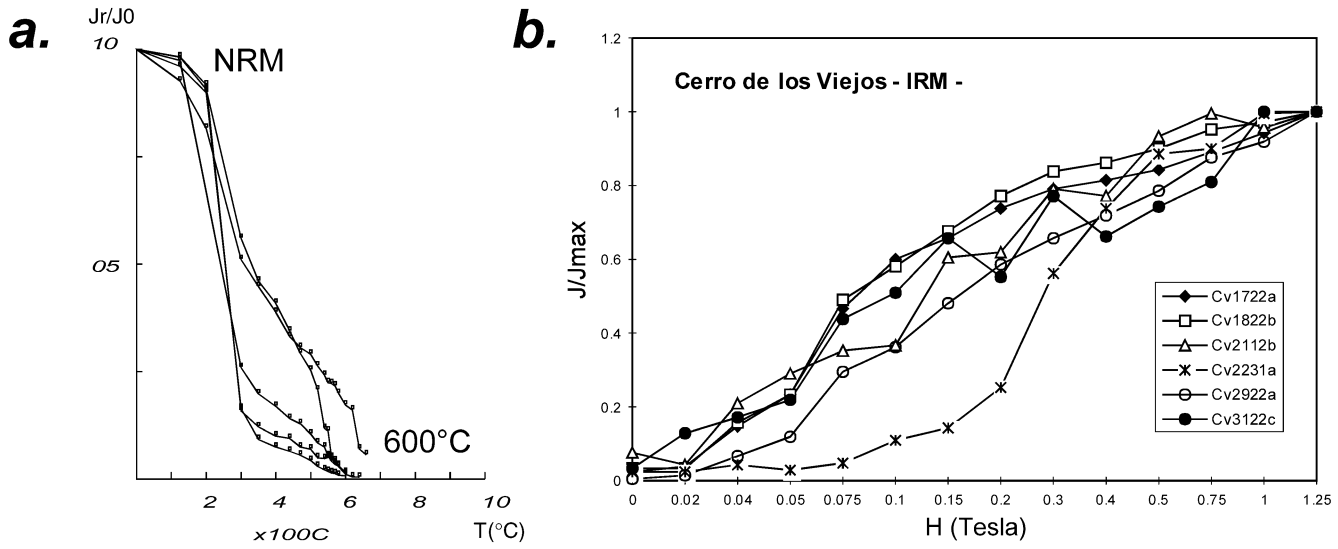

Fig. 8. (a) Demagnetization curves for typical specimens from Cerro de los Viejos. (b) Normalized isothermal remanent magnetization (IRM) acquisition curves.

oxides are both new generation euhedral magnetites as well as cataclased early magnetites.

6. Conclusions

The fabric of the Cerro de los Viejos gneiss contains two distinctive foliations, s_1 and s_2. S_1, the visible foliation, trends 146°/25°SW approximately. S_2, although secondary in terms of relative age and in degree of development, is the dominant foliation in terms of planar magnetic anisotropy, as shown by the strong clustering of K_{min} perpendicular to s_2. The anisotropy of AMS is mostly less than 3%. The thermal demagnetization curve of composite IRM indicates that much of the magnetization is carried by magnetite and possibly multi-domain titanomagnetite. In addition, the experiments of IRM acquisition showed that the carrier of the remanence includes also a high coercivity mineral, probably hematite.

The primary foliation s_1 formed during the main deformation in the area. The formation of the secondary foliation s_2 is obscured by the lack of exposures around the Cerro de los Viejos. However, it is clear that the area was subjected to more than one deformation episode. Investigation of adjacent areas in this part of the Samfrau belt may reveal the evolution of this part of Gondwana and its relation with Patagonia.

Acknowledgements

This paleomagnetic study is part of an external grant to R.N. Tomezzoli, supported by the CONICET-Argentina and Universidad de Buenos Aires, Departamento de Ciencias Geológicas. W.D. MacDonald acknowledges support through N.S.F. INT-9903915. H. Tickyj's participation was supported by PIP-CONICET 4329/96. Laboratory work was mainly performed at the Department of Geological Sciences, State University of New York at Binghamton, USA. We recognize special debts to E. Cristallini, for his invaluable collaboration during all phases of this work, and G. Bottessi for his collaboration in the field work. A. Goldstein of Colgate University and L. Brown of the University of Massachussets kindly provided access to essential equipment. Drs S. Neves, J. Bouchez and G. Borradaile are acknowledged for suggesting significant improvements to this paper. The computer software Estereográfica-GR (E.O. Cristallini) and APLOT10 modified by: B. Lienert were used in the analyses and graphics.

References

Aranguren, A., Cuevas, J., Tubía, J.M., 1996. Composite magnetic fabrics from *S–C* mylonites. Journal of Structural Geology 18, 863–869.

Benn, K., Ham, N.M., Pignotta, G.S., Bleeker, W., 1998. Emplacement and deformation of granites during transpression: magnetic fabrics of the Archean Sparrow pluton, Slave Province, Canada. Journal of Structural Geology 20, 1247–1259.

Borradaile, G.J., 1988. Magnetic susceptibility, petrofabrics and strain. Tectonophysics 156, 1–20.

Borradaile, G.J., Tarling, D.H., 1981. The influence of deformation mechanisms on magnetic fabrics in weakly deformed rocks. Tectonophysics 77, 151–168.

Borradaile, G.J., Henry, B., 1997. Tectonic applications of magnetic susceptibility and its anisotropy. Earth Sciences Review 42, 49–93.

Bouchez, J.L., Gleizes, G., 1995. Two-stage deformation of the Mont Louis–Andorra granite pluton (Variscan Pyrenees) inferred from magnetic susceptibility anisotropy. Journal of the Geological Society of London 152, 669–679.

Du Toit, A., 1927. A geological comparison of South America with South Africa. Carnegie Institute of Washington Publications 381, Washington, pp. 1–157.

Flinn, D., 1962. On folding during three dimensional progressive deformation. Journal of the Geological Society of London 118, 385–428.

Gleizes, G., Nédélec, A., Bouchez, J.L., Autran, A., Rochette, P., 1993. Magnetic susceptibility of the Mount Louis–Andorra ilmenite-type granite (Pyrenees): a new tool for the petrographic characterization and regional mapping of zoned granite plutons. Journal of Geophysical Research 98, 4317–4331.

Graham, J.W., 1954. Magnetic susceptibility, an unexploited element of petrofabric. Geological Society of American Bulletin 65, 1257–1258.

Jelinek, K., 1981. Characterization of the magnetic fabric of rocks. Tectonophysics 79, 63–67.

Jover, O., Rochette, P., Lorand, J.P., Maeder, M., Bouchez, J.L., 1989. Magnetic mineralogy of some granites from the French Massif Central: origin of their low-field susceptibility. Physics of the Earth and Planetary Interiors 55, 79–92.

Kay, S.M., Ramos, V.A., Mpodozis, C., Sruoga, P., 1989. Late Paleozoic to jurassic silicic magmatism at the Gondwana margin: Analogy to the Middle Proterozoic in North America? Geology 17: 324–328.

Linares, E., Llambías, E.J., Latorre, C.A., 1980. Geología de la Provincia de La Pampa, República Argentina y geocronología de sus rocas metamórficas y eruptivas. Revista de la Asociación Geológica Argentina 35, 87–146.

Lister, G.S., Snoke, A.W., 1984. *S–C* mylonites. Journal of Structural Geology 6, 617–638.

MacDonald, W.D., Ellwood, B.B., 1987. Anisotropy of magnetic susceptibility: sedimentological, igneous and structural-tectonic applications. Reviews of Geophysics 25, 905–909.

Nagata, T., 1961. Rock Magnetism. . 2nd ed.Maruzen, Tokyo 350pp.

Ramos, V.A., 1984. Patagonia: un continente paleozoico a la deriva? IX Cong. Geol. Argentino, Actas II, S.C. Bariloche, Buenos Aires, pp. 311–325.

Rapalini, A.E., Vizán, H., 1993. Evidence of intrapangaea movements in Gondwanaland. Comptes Rendus XII (I), 405–434.

Rochette, P., 1987. Magnetic susceptibility of the rock matrix related to magnetic fabric studies. Journal of Structural Geology 9, 1015–1020.

Tarling, D.H., Hrouda, F., 1993. The Magnetic Anisotropy of Rocks. Chapman & Hall, London 217pp.

Tickyj, H., 1999. Estructura y petrología del basamento cristalino de la región centro-sur de la provincia de La Pampa, Argentina. Tesis Doctoral. Universidad Nacional de La Plata, 228. La Plata. Unpublished.

Tickyj, H., Llambías, E.J., 1994. El gneis milonítico del Cerro de los Viejos (38°28′S–64°26′O), provincia de La Pampa, Argentina. Evidencia de un corrimiento en el Carbonífero Inferior. 7° Congreso Geológico Chileno II, 1239–1243.

Tickyj, H., Dimieri, L.V., Llambías, E.J., Sato, A.M., 1997. Cerro de los Viejos (38° 28′S–64° 26'O): cizallamiento dúctil en el sudeste de La Pampa. Revista de la Asociación Geológica Argentina 52 (3), 311–321.

Tomezzoli, R.N., 2001. Further palaeomagnetic results from the Sierras Australes fold and thrust belt, Argentina. Geophysical Journal International 147, 356–366.

Tomezzoli, R.N., Vilas, J.F., 1999. Palaeomagnetic constraints on age of deformation of the Sierras Australes thrust and fold belt. Geophysical Journal International 138, 857–870.

Trindade, R.I.F., Raposo, M.I.B., Ernesto, M., Siqueira, R., 1999. Magnetic susceptibility and partial anhysteretic remanence anisotropies in the magnetite-bearing granite pluton of Taurao, NE Brazil. Tectonophysics 314, 443–468.

Werner, T., Borradaile, G.J., 1996. Paleoremanence dispersal across a transpressed Archean terrain: deflection by anisotropy or by late compression?. Journal of Geophysical Research 101, 5531–5545.